Nanoplasmon-enabled macroscopic thermal management

SCIENTIFIC REPORTS

OPEN

SUBJECT AREAS:

SOLAR ENERGY AND PHOTOVOLTAIC TECHNOLOGY

NANOPHOTONICS AND PLASMONICS

CHARACTERIZATION AND ANALYTICAL TECHNIQUES

METAMATERIALS

Received
27 March 2013

Accepted
13 May 2014

Published
29 May 2014

Correspondence and requests for materials should be addressed to A.D. (alexd@chalmers.se)

Nanoplasmon-enabled macroscopic thermal management

Gustav Edman Jonsson, Vladimir Miljkovic & Alexandre Dmitriev

Department of Applied Physics, Chalmers University of Technology, Göteborg 41296, Sweden.

In numerous applications of energy harvesting via transformation of light into heat the focus recently shifted towards highly absorptive nanoplasmonic materials. It is currently established that noble metals-based absorptive plasmonic platforms deliver significant light-capturing capability and can be viewed as super-absorbers of optical radiation. Naturally, approaches to the direct experimental probing of *macroscopic* temperature increase resulting from these absorbers are welcomed. Here we derive a general quantitative method of characterizing heat-generating properties of optically absorptive layers via macroscopic thermal imaging. We further monitor macroscopic areas that are homogeneously heated by several degrees with nanostructures that occupy a mere 8% of the surface, leaving it essentially transparent and evidencing significant heat generation capability of nanoplasmon-enabled light capture. This has a direct bearing to a large number of applications where thermal management is crucial.

Practical thermal platforms for solar energy harvesting and manipulation of thermal radiation are necessarily highly absorbing, but also affordable and scalable. Nanoplasmonic metamaterial absorbers[1–7] offer a route towards low material consumption and compact designs while maintaining large optical cross-sections[8–11]. They exploit the collective oscillations of electrons in metallic nanostructures - localized plasmons - for the highly efficient coupling of light. In the same time, individual plasmon nanostructures in these materials act collectively as an effective absorbing layer, i.e., a metasurface. The emerging field of thermoplasmonics then addresses applications of light-heated plasmonic nanostructures in photothermal therapeutics and drug release[1,12–15], thermal optical data storage[16], enhanced catalysis[4,17,18], magnetic recording[19,20], solar thermal energy harvesting[6,21–23] and optoelectronics[24,25].

Whereas up to now the focus is on intricate design of nanoplasmonic metamaterials units, often by advanced electromagnetic simulations and highly demanding nanofabrication methods such as electron-beam lithography, recent advances in nanofabrication have led to simple and thereby cheap large-scale manufacturing methods of light absorbing plasmonic metasurfaces[26,27]. These approaches utilize amorphous arrangements of individual nanoplasmonic structures (meta-atoms) with simple geometries, which as a whole develop desired collective absorptive properties. When developing realistic light absorbing nanoplasmonic systems, optimization primarily focuses on the size, shape and material composition of the individual particles. While local plasmon-enabled thermal gradients, confined to the nanoscale, are well-documented in these systems[28–35], large-scale (i. e., *macroscopic*) thermal effects due to plasmons are also of strong interest since their importance in e.g. catalysis has been demonstrated[36,37]. In the wake of the development of macroscopic plasmon metamaterial absorbers that aim, for example, at wafer-scale solar thermal harvesting, the comprehensive experimental characterization of such thermal effects comes handy.

The prime aim when developing absorbing plasmonic architectures is to enhance the non-radiative decay of the excited nanoplasmons. This is typically done by reducing the size of plasmonic nanoparticles or by changing the dielectric function of the material[38]. Although noble metal nanoparticles of Au or Ag are widely used in plasmon metamaterials due to their well-pronounced resonances in the visible and near-IR, they might not be the best choice as absorbing platforms. Under white light or solar illumination plasmonic nanostructures having markedly lower but instead spectrally broader absorption may be equal to or even surpassing Au-based superabsorbers.

Results

We utilize simple large-area bottom-up nanofabrication method – hole mask colloidal lithography[27] - to prepare absorbing plasmonic metasurfaces, composed of amorphous arrays of Ni or Au nanodisks that are 20 nm high and nominally 110 nm in diameter (Figure 1a). Figure 1b shows the absorption in these two types of nanoplas-

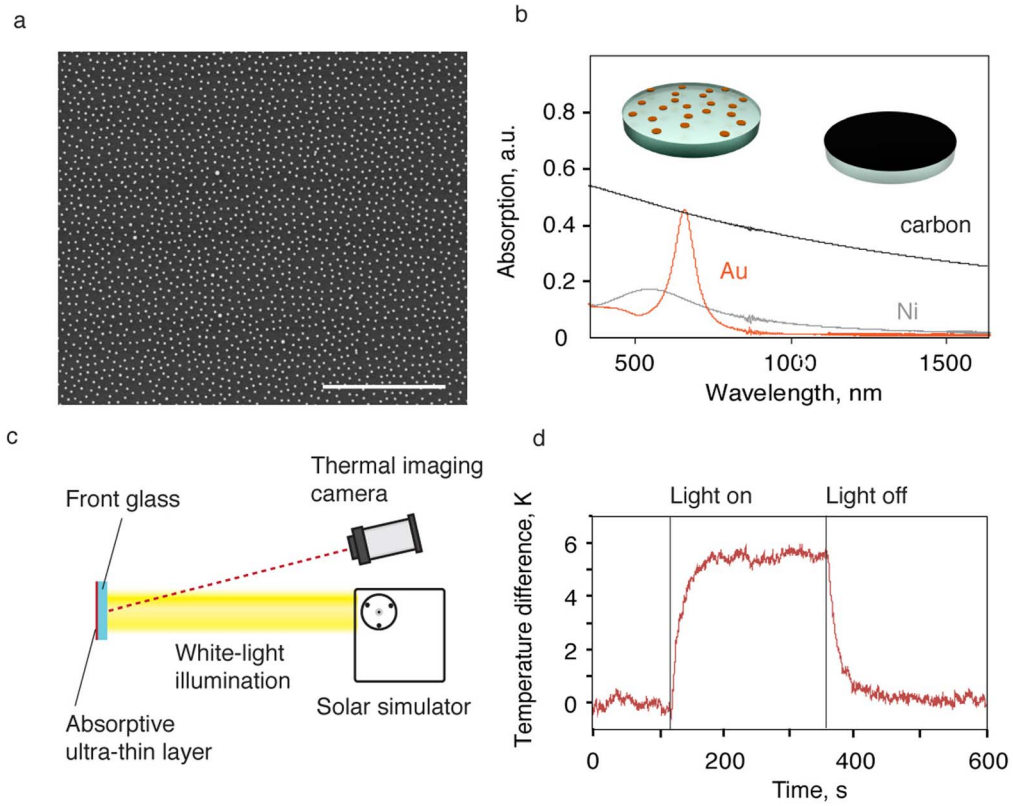

Figure 1 | (a) SEM micrograph of a plasmonic metasurface – amorphous arrangement of Ni nanodisks (scale bar – 5 μm); (b) Absorption spectra of Au and Ni nanodisks and of carbon thin film of the same thickness as the height of the plasmon particles. Insets schematically show both types of absorbing platforms; (c) Experimental setup for measuring temperature and (d) a typical temperature response.

monic metasurfaces, along with that of a carbon film of equal thickness that we use as the absorption benchmark. Au nanodisks layer shows strong and spectrally narrow absorption peak at the plasmon resonance. The Ni nanodisks system displays broader and generally lower absorption as a result of the shorter plasmon lifetime that is due to the strong electron-lattice coupling in Ni.

Although optical spectroscopy gives straightforward quantification of light absorption in these metasurfaces, it understandably does not address the crucial information on the ability to generate elevated temperature *at a macroscale* due to such absorption. With the current study we put forward a new modality of characterizing macroscopic absorbing metasurfaces – that is, via their temperature increase upon illumination. We naturally consider that all absorbed light eventually transforms into heat in these systems. With this measuring modality we illuminate the surface with the solar simulator to benefit from potential omnichromatic absorption of the practical metamaterial absorber and track the resulting surface temperature with a thermal camera (Figure 1c, further experimental details can be found in Methods section). Due to identical thermal radiation emissivity properties of the substrates (as opposed to the studied metasurfaces), we arrange the measuring system in a way that the ultra-thin absorbing plasmon metasurface is positioned at the backside of the sample and glass slide is facing light source and the thermal camera (c.f., Fig. 1c). The temperature is further obtained by averaging the camera reading from the center part of the sample at which the illumination is homogeneous (typically, about 1 cm^2) first without the illumination (1 to 2 min), then with light on and reaching temperature saturation (about 3 min), and finally after light is off tracking the cooling-off kinetics (further 3 to 4 min). The result for the amorphous array of Au nanodisks as an absorber is shown in Figure 1d, with vertical axis presenting the difference to the temperature in the dark (room temperature). At this point one clearly marks the macroscopic temperature effect due to the presence of plasmon metasurface and overall sample temperature increase up to 5–6 degrees. We note here that temperature evolution in Fig. 1d concerns the entire system – that is, plasmon metasurface, glass slide and the surrounding air altogether. Specifically, at the point of temperature saturation, a thermal equilibrium exists between these three media, and the temperature gradients are established within the glass substrate - the hottest being plasmon metasurface layer.

To quantify the actual absorbed power we employ a simple numerical method. First we assume that, since it is thin and fully illuminated, the substrate has a homogeneous temperature. Any change of this temperature is directly proportional to a change of energy, per unit area, through the density of mass, specific heat, and thickness of the substrate. Differentiating this energy with respect to time gives the net thermal flux, heating (or cooling) the substrate. In principle the substrate has a constant positive (i.e. heating up) flux of heat coming from the absorbing metasurface upon solar illumination. A negative heat flux is present when the substrate has a higher temperature than its surroundings. This negative flux is proportional to the temperature difference between the sample and its surroundings through two main terms: convective and radiative heat transfers. The convective term is a function of the temperatures to the power of unity, the radiative - to the power of four. However, since we are interested only in a small temperature window far from absolute zero, the radiative term can also be assumed to be linear with respect to the temperature inside this measurement window. Now, plotting the thermal flux against the substrate temperature displays two regions of interest (Figure 2a, left): the data corresponding to heating and cooling of the substrate, respectively. Calculating the offset between linear fits to the heating and cooling data earns the heating power. Figure 2a schematically outlines the general procedure of extracting the absorbed power with the given system (the actual fit

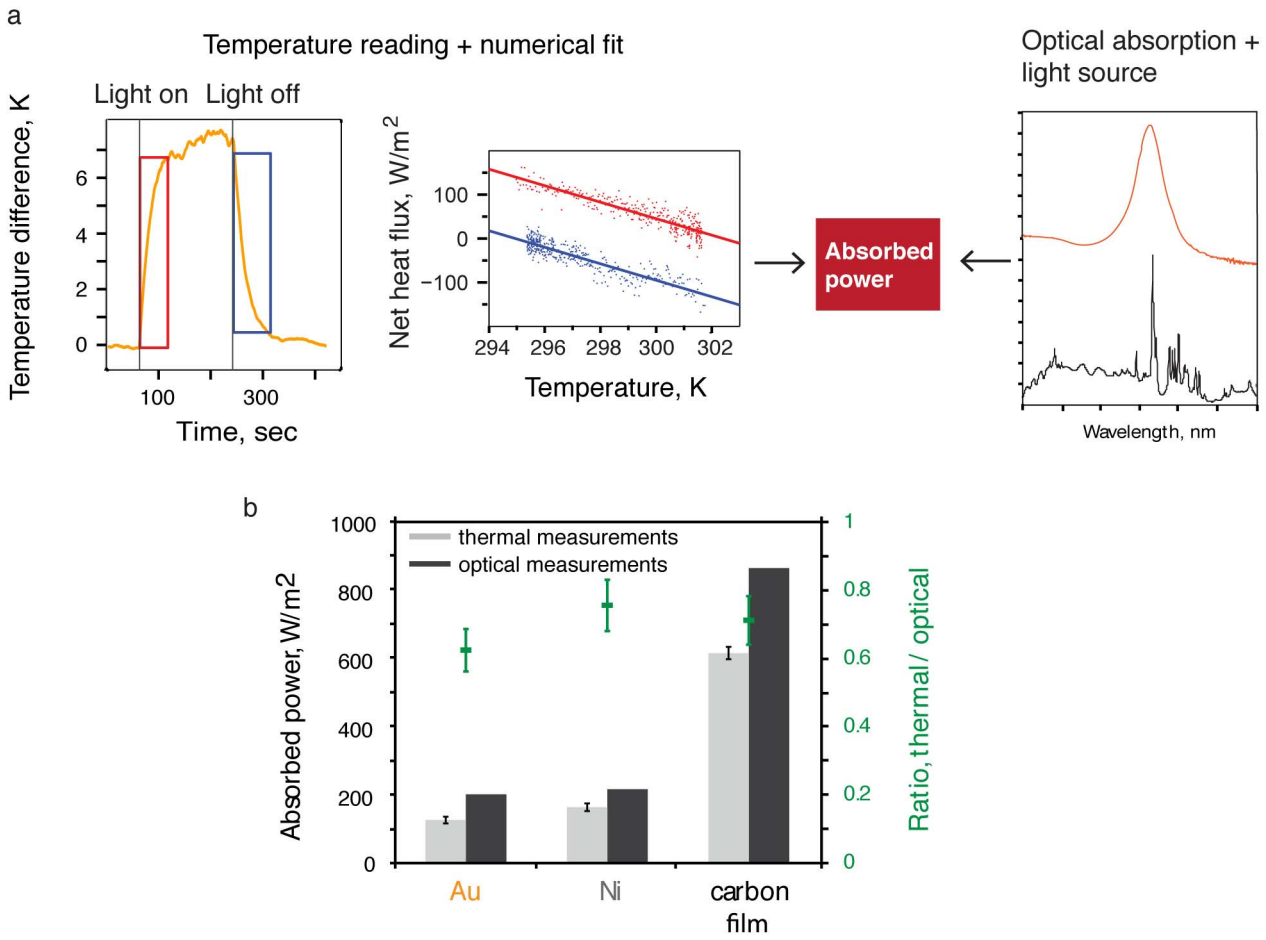

Figure 2 | (a) Schematic outline of the absorbed power measurement with two complimentary methods – temperature reading, fitted with numerical model (left) and optical absorption, combined with the emission spectrum of the light source (right). Net heat flux in (a) corresponds to the time-differentiated temperature in the blue and red highlighted rectangular regions of the temperature-vs.-time plot, multiplied by the factor for temperature-to-energy conversion. (b) Absorbed power from thermal (light grey) and optical (dark grey) measurements (error bars shown for thermal measurements), green bars mark the ratio between the two (right axis).

to experimental data is shown, Figure 2a, left) and cross-referencing it to the measured optical absorption (Figure 2a, right). The absorbed powers for three systems, extracted both from the temperature data (light grey) and optical absorption (dark grey), are presented in Figure 2b. Here we compare two nanoplasmonic platforms (amorphous arrays of Au or Ni nanodisks) and carbon film. For completeness we also plot the ratio of the two (green bars, with the corresponding vertical axis to the right). The latter visually confirms the consistency between the thermally derived absorption and the optically measured one in all three systems. In order to keep the generality of the approach and maintaining the robustness of the absorbed power extraction against the particularities of the exact solar thermal system under consideration (i.e., exact substrate thickness, absorbing metamaterials composition etc.), we rely on the best fit of the experimental temperature data that the model provides. This, in general, underestimates the extracted absorbed power as verified by the direct optical absorption measurements (c.f Fig. 2b). Furthermore, the ratio of thermal-to-optical retrieved absorption power varies between the samples. This variation is largely due to uncertainties in the optical absorption measurements. The optical absorption is measured with an illumination spot size of only a few mm^2. Slight variations in particle coverage over the sample surfaces therefore have significant impact on the measurement result. In contrast, the thermal method averages absorption over the larger area, which makes it less sensitive to such inhomogeneity.

We further establish that the quantitative aspects of the absorptive properties of a given thin functional layer, in principle, of unknown composition and morphology can be directly extracted from the thermal data. For example, comparing absorptive Au metamaterial surface with carbon film, one concludes that the carbon film absorbs 4.5 times more than Au metamaterial. In our case this is also directly verified by the measured optical absorbance for all three systems. Excitingly, if the morphology of the absorptive layer is known (i.e., film thickness and/or nanostructures size and coverage, so the overall content of the absorptive material is quantified) - straightforward comparison of the heat generation ability of these ultrathin macroscopic functional layers can be made. In our case, normalizing the thermal power on materials coverage both for nanoplasmonic metasurfaces and carbon film, we estimate nanoplasmonic systems to deliver 3.4 times higher absorption/thermal power per surface unit given that they have a surface coverage of 8 per cent.

Now that we outlined the method to correlate total broadband absorption and thermal effects, we turn back to the plasmon-enabled heat-generation platforms to mark the possible route towards an optimal plasmonic 'solar heater'. As mentioned earlier, gold- and silver-based plasmonic nanoarchitectures typically display strong and spectrally well-defined region of light absorption that is linked to the plasmon resonance. By contrast, metals like Ni present markedly broader plasmon feature in absorption due to higher ohmic losses. We use the latter property to design a simple plasmonic solar

temperature system that favorably compares to structurally identical one, but made of Au. Namely, we use presented method to compare the absorbed power in amorphous arrays of Au and Ni nanoellipses of three sizes: (i) 80 × 60 nm, (ii) 112 × 60 nm and (iii) 140 × 100 nm. Figures 3a–c compare longitudinal and transversal optical absorption of Au (right panels) and Ni (left panels) nanoellipses. (the overall array morphology for both materials is depicted in Fig. 3d). Even though both longitudinal and transversal peak optical absorption in Ni systems are visibly lower (compare left and right panels for all nanoellipses sizes), significant spectral broadening of the absorption in Ni makes total areas under the peaks, which in this sense correspond to the actual absorption over the entire solar spectral range, noticeably larger (c.f. the solar irradiance schematics in Figs. 3 a–c at the background). In general, larger plasmonic particles are known to have larger scattering cross-sections than smaller ones[39], thereby loosing in their absorption cross-section. Due to their strongly damped plasmon resonances, Ni nanostructures deviate from this generic trend. This fact directly reports in the thermally measured data (Figure 3e), where upon non-polarized solar simulator illumination 100 × 140 nm Ni nanoellipses generate 30% more heat than corresponding nanostructures of Au. Note that thermal-to-optical absorbed power ratio tends to be the same as in the case of Ni and Au nanodisks and the carbon film (compare the thermal-to-optical ratios in green on Figs. 2b and 3e). Overall, the comparison of differently shaped and sized nanostructures of various materials signals that Ni-based plasmonic absorbers would potentially deliver appreciably large and spectrally broad heat-generation capability in practical applications.

Efficiency under oblique incident light is another practically important property of a solar absorber. In Figure 4 we present generated heat from nickel nanodisks and nanoellipses, illuminated with light incident at 0, 30 and 60 degrees off normal, with the plasmon metasurface at the backside (i.e., in the same measuring geometry as in all discussed cases here, see Figure 1c). Figure 4 presents data for nanoellipses oriented both with long and short axes in the plane of incidence. Interestingly, the efficiencies of the thermal power generation by the plasmon metasurfaces at oblique illumination are slightly higher than what can be expected from the regular photovoltaics cells in the similar light conditions. In fact, in photovoltaics the decrease in insolation, with a cosine dependence on the angle of incidence, is one of the main causes for the lowered resulting efficiencies[40]. Cosine dependence dictates an insolation loss of 50 per cent at 60 degrees angle of incidence from normal. Plasmon metasurfaces (both of nanodisks and nanoellipses) display about 30% decrease in the absorbed power generation when the illuminating light changes incidence from 0 to 60 degrees from normal, thus positively comparing with the relevant numbers in photovoltaics. It would seem that the increased optical path upon the grazing incidence, possibly combined with the waveguiding modes in the glass substrate, positively contributes to the absorptive ability of plasmon thermal metasurfaces.

These results bring forward the potential of other 'non-conventional' plasmonic materials – such as Pd, Pt, Co and others – as plasmon-enabled thermal metamaterial platforms for solar energy harvesting[41,42]. They typically feature very moderate absolute absorption in a broad spectral range (c.f., Fig. 1b) that also comfortably covers solar radiation spectrum. This leaves macroscopic areas that are functionalized with thermal plasmon nanostructures essentially transparent. In the same time, these nanostructures provide superior heat-generation ability. With the simultaneous access to design and affordable fabrication of truly large-scale thermal plasmonic metasurfaces from these materials, the concepts of plasmon-enabled heating might spill into applications of thermal surfaces, for example, in energy-efficient technologies for construction and industrial design. Another exciting prospect is in thermal plasmonics of nanoferromagnets for the manipulation of magnetic order. Indeed, plasmon-induced temperature effects are currently actively explored with magnetoplasmonics[19,20] With the current work we show that Ni as efficient nanoplasmon heat antenna[43,44] has substantial heat-generation ability and thus might find direct use in promoting strong nanoscale temperature gradients for effective magnetization manipulation.

Discussion

Summarizing, we devised a modality to comprehensively characterize the absorbing and heat-generating ability of various ultra-thin absorbers, most importantly including plasmon-enabled macroscopic absorbing metasurfaces. It is also very appealing that the method allows for quantitative comparison of fundamentally different absorbing systems. Further, we used the method to mark the possible route towards potentially high-efficient omnichromatic and omnidirectional plasmon absorbers that utilize Ni rather than Au. It is also appealing to exploit high spectral tunability of various plasmonic nanostructures to address various spectral regions for the most efficient heat power generation with such metasurfaces. There is a wide and immediate implication of these findings – that is, this work provides very simple tool to increase the credibility of the studies addressing super-absorbing platforms - metallic, dielectric or semiconducting. It aids to make a direct step from claiming highly absorptive properties to the actual proof of the resulting increased temperature. Specifically, studies using a spectrally variable monochromatic light source instead of a solar simulator would in addition allow wavelength-resolved measurements of the actual heat generation.

All these powerful features open up new possibilities for the reliable evaluation and practical implementation of ultra-thin metamaterial superabsorbers in photocatalysis, energy-efficient design, thermal magnetization control and other applications where thermal management is important.

Methods

Plasmonic nanodisks and nanoellipses were prepared with the hole-mask colloidal lithography process as it is described elsewhere[27]. Polysterene particles with 110 nm diameter were used to fabricate the masks for the disks. 60, 80 and 100 nm particles were used for the masks of 84 × 60, 112 × 80 and 140 × 100 nm ellipses respectively. The thickness of all structures was 20 nm. 0.21 mm thick circular borosilicate cover glasses with 25 mm diameter (D 263 M, Menzel-Gläser) were used as substrates for the disks and 0.4 mm thick 15 × 15 mm cover glasses of the same type were used for the ellipses. The samples were entirely homogeneously covered by plasmonic nanoparticles. Samples with carbon thin films were prepared by e-beam evaporation of carbon on 0.5 mm thick fused silica substrates followed by annealing in Ar atmosphere at 800°C for 10 min.

Optical absorption measurements were done using Cary 5000 spectrophotometer [Varian] with an integrating sphere [DRA 2500, Varian] equipped with the small-spot kit. The samples were either positioned using the center mount sample holder or placed at the reflectance- and transmission ports alternately. In both cases specularly reflected light was included. The baselines were recorded with an empty sample holder in place. SEM micrographs of the plasmonic nanostructures were obtained from the same samples as the other measurements were made on using a Quanta 200 FEG ESEM, FEI. Particle sizes and number densities were determined from the micrographs using the software ImageJ 1.44o.

Time resolved photo-induced surface temperatures of the samples were measured with a setup consisting of a solar simulator [ss150, Sciencetech – see the output spectrum in Appendix] as light source, thermal cameras A20, FLIR. (for nanodisks samples and carbon films) and A645 sc, FLIR (used for nanoellipse) were used to monitor the sample temperature and a sample holder with the sample. The samples were positioned in the center of the solar simulator light beam at normal angle to ensure homogeneous illumination in the center part of the samples. The intensity of light was calibrated to 2 suns (2000 W/m^2) using a photodiode [Sciencetech]. The absorbing metamaterial side of the sample (i.e. the backside) was faced away from the light source, and the thermal camera was directed towards the front side of the sample at an angle large enough for the IR-radiation specularly reflected by the sample into the camera to be that of the ambient environment and not from the camera itself or the solar simulator. The ambient environment has a known and constant emission as opposed to the thermal camera or the solar simulator, thus allowing reliable thermal measurements. Measuring the temperature of the samples at an angle does not affect the reading since both the thermal emission and projected area have a cosine dependence on the angle of observation. The thermal camera in principle calculates the temperature from measured radiosity (radiated power per unit area) and since

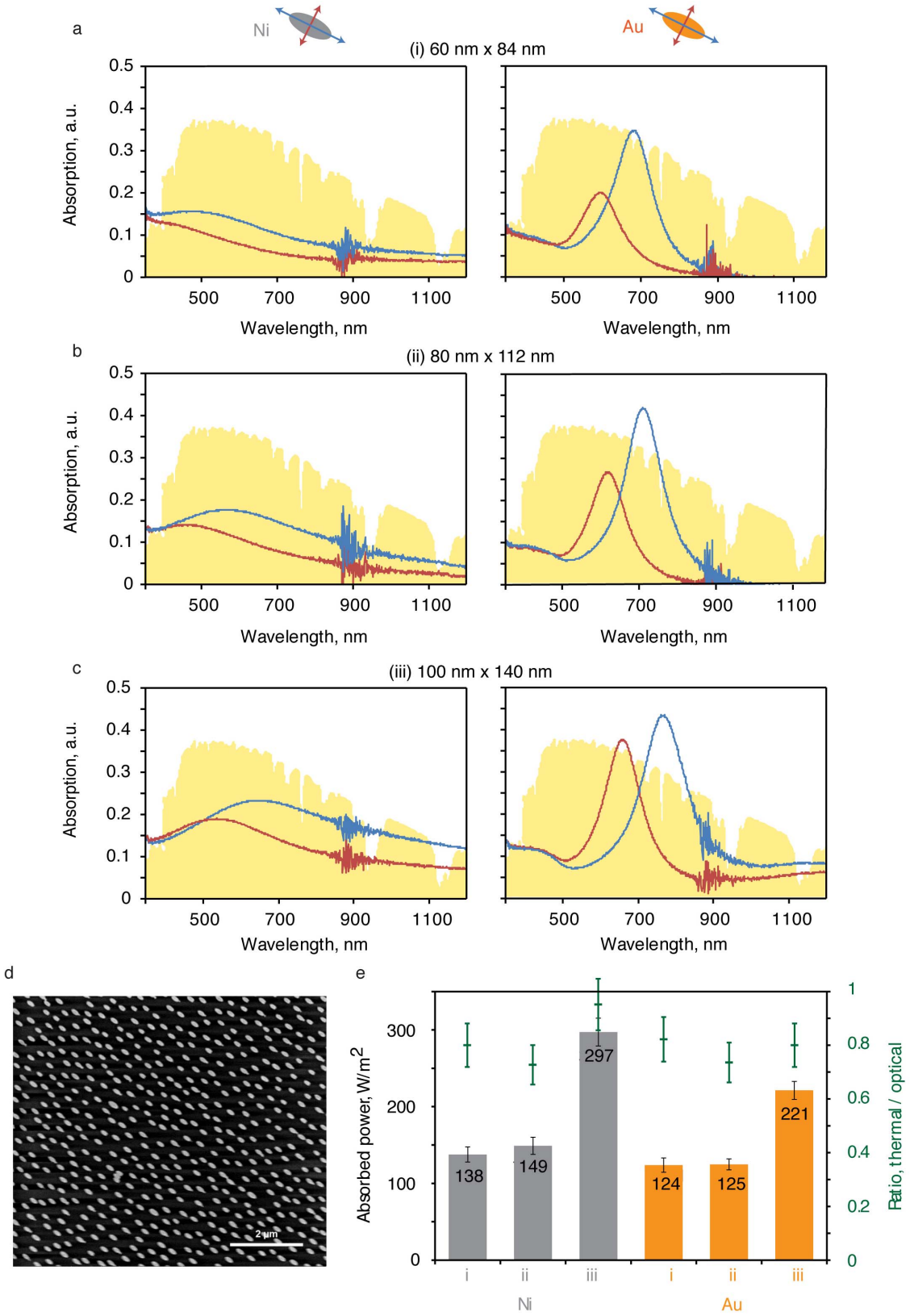

Figure 3 | Longitudinal (blue) and transversal (red) optical absorption in Ni (left) and Au (right) ellipses of sizes (a, i) 60 × 84 nm, (b, ii) 80 × 112 nm and (c, iii) 100 × 140 nm. nanoellipses. Schematics of the mutual orientation of nanoellipses axes and the polarization of the incoming light in absorption measurements. Solar irradiance (not to scale) is shown schematically in the background as a guide. (d) SEM image of a typical nanoellipses arrangement, prepared by HCL. (e) Thermally measured absorbed power in Au (orange) and Ni (grey). Ratios to spectroscopically-retrieved absorbed power are shown with green bars (right axis). Error bars on absorption data indicate the standard deviation of at least 3 measurements on the same sample. Error bars on thermal-to-optical absorbed power ratios indicate 9% deviation from the weighted average.

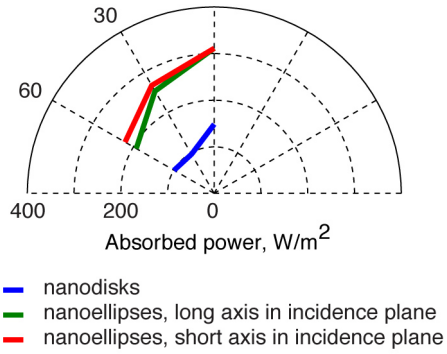

Figure 4 | Absorbed power (measured with the thermal camera) for Ni nanodisks (blue) and nanoellipses (red and green) with light incident at 0, 30 and 60 degrees from normal. Nanoellipses are oriented with long (green) or short (red) axes in the plane of incidence.

both the perceived area and the perceived radiosity scales equally with respect to observing angle the both effects cancel each other.

The emissivity of the sample front side (glass surface) was verified by heating the substrate above 50°C and measuring its temperature using a thin k-type thermocouple with its hot junction adhered to the substrate by Ag-glue and its cold junction kept at a controlled 0°C. At the same time the temperature of the substrate was measured with the thermal camera. As the temperature readings were equal, the correct emissivity can be recorded in the real experiments. To reduce the heat dissipated from the sample via thermal contacts, the sample holder balanced the sample between two razorblade edges and a sharpened wire tip.

The thermal power delivered to the substrate was estimated using a MatLab script. Curve fitting was done using the MatLab internal function 'fit'. Material properties consisted of the density of mass and the specific heat capacity. Values for the cover glasses were provided by the manufacturer. Fused silica values were taken from the literature[45].

1. Jain, P. K., El-Sayed, I. H. & El-Sayed, M. A. Au nanoparticles target cancer. *Nano Today* **2**, 18–29 (2007).
2. Wu, T. H. *et al.* Photothermal nanoblade for large cargo delivery into mammalian cells. *Anal. Chem.* **83**, 1321–1327 (2011).
3. Donner, J. S., Baffou, G., McCloskey, D. & Quidant, R. Plasmon-assisted optofluidics. *ACS Nano* **5**, 5457–5462 (2011).
4. Cao, L., Barsic, D. N., Guichard, A. R. & Brongersma, M. L. Plasmon-assisted local temperature control to pattern individual semiconductor nanowires and carbon nanotubes. *Nano Lett.* **7**, 3523–3527 (2007).
5. Maity, S., Downen, L. N., Bochinski, J. R. & Clarke, L. I. Embedded metal nanoparticles as localized heat sources: An alternative processing approach for complex polymeric materials. *Polymer* **52**, 1674–1685 (2011).
6. Neumann, O. *et al.* Solar Vapor Generation Enabled by Nanoparticles. *ACS Nano* **7**, 42–49 (2012).
7. Aubry, A. *et al.* Plasmonic Light-Harvesting Devices over the Whole Visible Spectrum. *Nano Lett.* **10**, 2574–2579 (2010).
8. Sondergaard, T. *et al.* Plasmonic black gold by adiabatic nanofocusing and absorption of light in ultra-sharp convex grooves. *Nat. Commun.* **3**, 969 (2012): DOI 10.1038/ncomms1976 (2012).
9. Atwater, H. A. & Polman, A. Plasmonics for improved photovoltaic devices. *Nature Mater.* **9**, 205–213 (2010).
10. Teperik, T. V. *et al.* Omnidirectional absorption in nanostructured metal surfaces. *Nature Photon.* **2**, 299–301 (2008).
11. Aydin, K., Ferry, V. E., Briggs, R. M. & Atwater, H. A. Broadband polarization-independent resonant light absorption using ultrathin plasmonic super absorbers. *Nat. Commun.* **2**, 517 (2011): DOI 10.1038/ncomms1528 (2011).
12. Hirsch, L. R. *et al.* Nanoshell-mediated near-infrared thermal therapy of tumors under magnetic resonance guidance. *Proc. Natl. Acad. Sci. USA* **100**, 13549–13554 (2003).
13. Huschka, R. *et al.* Light-Induced Release of DNA from Gold Nanoparticles: Nanoshells and Nanorods. *J. Am. Chem. Soc.* **133**, 12247–12255 (2011).
14. Loo, C., Lowery, A., Halas, N. J., West, J. & Drezek, R. Immunotargeted nanoshells for integrated cancer imaging and therapy. *Nano Lett.* **5**, 709–711 (2005).
15. Pissuwan, D., Valenzuela, S. M. & Cortie, M. B. Therapeutic possibilities of plasmonically heated gold nanoparticles. *Trends Biotechnol.* **24**, 62–67 (2006).
16. Wang, L. & Li, B. W. Thermal Memory: A Storage of Phononic Information. *Phys. Rev. Lett.* **101**, 267203; DOI http://dx.doi.org/10.1103/PhysRevLett.101.267203 (2008).
17. Adleman, J. R., Boyd, D. A., Goodwin, D. G. & Psaltis, D. Heterogenous Catalysis Mediated by Plasmon Heating. *Nano Lett.* **9**, 4417–4423 (2009).
18. Christopher, P., Xin, H. & Linic, S. Visible-light-enhanced catalytic oxidation reactions on plasmonic silver nanostructures. *Nature Chem.* **3**, 467–472 (2011).
19. Challener, W. A. *et al.* Heat-assisted magnetic recording by a near-field transducer with efficient optical energy transfer. *Nature Photon.* **3**, 220–224 (2009).
20. Stipe, B. C. *et al.* Magnetic recording at 1.5 Pb m(-2) using an integrated plasmonic antenna. *Nature Photon.* **4**, 484–488 (2010).
21. Neumann, O. *et al.* Compact solar autoclave based on steam generation using broadband light-harvesting nanoparticles. *Proc. Natl. Acad. Sci. USA* **110**, 11677–11681 (2013).
22. Lee, B. J., Park, K., Xu, L. & Walsh, T. Radiative Heat Transfer Analysis in Plasmonic Nanofluids for Direct Solar Thermal Absorption. *J. Sol. Energ.-T ASME* **134**, 021009–021009 (2012).
23. Molesky, S., Dewalt, C. J. & Jacob, Z. High temperature epsilon-near-zero and epsilon-near-pole metamaterial emitters for thermophotovoltaics. *Opt. Express* **21**, A96–A110 (2013).
24. Dyer, G. C., Aizin, G. R., Reno, J. L., Shaner, E. A. & Allen, S. J. Novel Tunable Millimeter-Wave Grating-Gated Plasmonic Detectors. *IEEE J. Sel. Top. Quant.* **17**, 85–91 (2011).
25. Vicarelli, L. *et al.* Graphene field-effect transistors as room-temperature terahertz detectors. *Nature Mater.* **11**, 865–871 (2012).
26. Moreau, A. *et al.* Controlled-reflectance surfaces with film-coupled colloidal nanoantennas. *Nature* **492**, 86–89 (2012).
27. Fredriksson, H. *et al.* Hole-mask colloidal lithography. *Adv. Mater.* **19**, 4297–4302 (2007).
28. Baffou, G., Girard, C. & Quidant, R. Mapping heat origin in plasmonic structures. *Phys. Rev. Lett.* **104**, 136805 (2010).
29. Baffou, G., Kreuzer, M. P., Kulzer, F. & Quidant, R. Temperature mapping near plasmonic nanostructures using fluorescence polarization anisotropy. *Opt. Express* **17**, 3291–3298 (2009).
30. Baffou, G., Quidant, R. & García De Abajo, F. J. Nanoscale control of optical heating in complex plasmonic systems. *ACS Nano* **4**, 709–716 (2010).
31. Baffou, G., Quidant, R. & Girard, C. Heat generation in plasmonic nanostructures: Influence of morphology. *Appl. Phys. Lett.* **94**, 153109 (2009).
32. Chen, X., Chen, Y., Yan, M. & Qiu, M. Nanosecond photothermal effects in plasmonic nanostructures. *ACS Nano* **6**, 2550–2557 (2012).
33. Honda, M., Saito, Y., Smith, N. I., Fujita, K. & Kawata, S. Nanoscale heating of laser irradiated single gold nanoparticles in liquid. *Opt. Express* **19**, 12375–12383 (2011).
34. Garnett, E. C. *et al.* Self-limited plasmonic welding of silver nanowire junctions. *Nature Mater.* **11**, 241–249 (2012).
35. Boyer, D., Tamarat, P., Maali, A., Lounis, B. & Orrit, M. Photothermal imaging of nanometer-sized metal particles among scatterers. *Science* **297**, 1160–1163 (2002).
36. Yen, C. W. & El-Sayed, M. A. Plasmonic Field Effect on the Hexacyanoferrate (III)-Thiosulfate Electron Transfer Catalytic Reaction on Gold Nanoparticles: Electromagnetic or Thermal? *J. Phys. Chem. C* **113**, 19585–19590 (2009).
37. Alejo, C. J. B., Fasciani, C., Grenier, M., Netto-Ferreira, J. C. & Scaiano, J. C. Reduction of resazurin to resorufin catalyzed by gold nanoparticles: dramatic reaction acceleration by laser or LED plasmon excitation. *Catal. Sci. Technol.* **1**, 1506–1511 (2011).
38. Bohren, C. F. & Huffman, D. R. *Absorption And Scattering Of Light By Small Particles* (Wiley, New York, 1983).
39. Langhammer, C., Kasemo, B. & Zoric, I. Absorption and scattering of light by Pt, Pd, Ag, and Au nanodisks: Absolute cross sections and branching ratios. *J Chem Phys* **126**, 267203; DOI http://dx.doi.org/10.1063/1.2734550 (2007).
40. Seshan, C. Cell Efficiency Dependence on Solar Incidence Angle. Paper presented at *Photovoltaic Specialists Conference (PVSC), 2010 35th IEEE*, Honolulu, HI; Publisher: IEEE; DOI: 10.1109/PVSC.2010.5616340 (June 20–25, 2010).
41. Wadell, C., Antosiewicz, T. J. & Langhammer, C. Optical Absorption Engineering in Stacked Plasmonic Au-SiO2-Pd Nanoantennas. *Nano Lett.* **12**, 4784–4790 (2012).
42. Antosiewicz, T. J., Apell, S. P., Wadell, C. & Langhammer, C. Absorption Enhancement in Lossy Transition Metal Elements of Plasmonic Nanosandwiches. *J. Phys. Chem. C* **116**, 20522–20529 (2012).
43. Chen, J. N. *et al.* Plasmonic Nickel Nanoantennas. *Small* **7**, 2341–2347 (2011).
44. Bonanni, V. *et al.* Designer Magnetoplasmonics with Nickel Nanoferromagnets. *Nano Lett.* **11**, 5333–5338 (2011).
45. Bansal, N. P. & Doremus, R. H. *Handbook Of Glass Properties* (Academic Press, Orlando, 1986).

Acknowledgments

We acknowledge Raja Sellappan (Chalmers) for providing the samples with carbon films. We also acknowledge Henrik Frederiksen (Chalmers) for his support in nanofabrication. This work is supported by the Swedish Foundation for Strategic Research (SSF) through RMA08-0109. AD acknowledges the Swedish Research Council. VM acknowledges the support from EU FP7 project "PRIMA" – 248154 and EU FP7 project 'PhotoNVoltaics' – 309127.

Author contributions

G.E.J. and A.D. wrote the manuscript, prepared the figures and planned the experiments. G.E.J. performed the experiments G.E.J. and V.M. did the numerical simulation. All authors have reviewed the manuscript.

Additional information

Supplementary information accompanies this paper at http://www.nature.com/scientificreports

Competing financial interests: The authors declare no competing financial interests.

How to cite this article: Jonsson, G.E., Miljkovic, V. & Dmitriev, A. Nanoplasmon-enabled macroscopic thermal management. *Sci. Rep.* **4**, 5111; DOI:10.1038/srep05111 (2014).